



A Novel System Architecture for Small-Scale Motion Sensing Exploiting 5G mmWave Channels

Simon Häger¹, Stefan Böcker¹, Shahin Jamali², Thomas Reinsch², and Christian Wietfeld¹

¹Communication Networks Institute (CNI), TU Dortmund University, Dortmund, Germany

²Fraunhofer IEG, Fraunhofer Research Institution for Energy Infrastructures and Geothermal Systems, Bochum, Germany

E-mail: {Simon.Haeger, Stefan.Boecker, Christian.Wietfeld}@tu-dortmund.de, {Shahin.Jamali, Thomas.Reinsch}@ieg.fraunhofer.de

Abstract—Cellular networks have become a globally available infrastructure which allows for a wide range of new services beyond communications, especially when the wireless channel itself is considered as a versatile sensor. This work illustrates that parts of the envisioned 6G sensing capabilities can already be realized in current networks, i.e. ground motion detection and infrastructure monitoring. Using 3D ray-tracing, we show that 5G mmWave can offer small-scale mobility tracking with sub-10 μm accuracy by exploiting pencil beam orientation and channel state information (CSI) phase information. Complementing current sensing platforms for ground motion detection and infrastructure monitoring, we outline present and future potentials of the proposed system, e.g. support for large numbers of commercial-off-the-shelf (COTS) monitoring devices available at low cost. Overall, this enables sustainable environmental motion monitoring reusing existing 5G infrastructure and, moreover, provision of public safety and disaster relief services.

I. INTRODUCTION

Sensing-based services are envisioned as a key feature of beyond 5G cellular networks [1] and will be enabled by introducing inherent radar-like capabilities, thus making future networks perceptive of their environment [2]. While it is an interesting area of research to reuse this data in order to enhance network operation [3], in particular for handover and mmWave beam management, the key incentive for network operators will be the many novel use cases opening up new revenue streams, e.g. positioning with prediction capabilities and sensing-assisted traffic. However, realization of this 6G concept will take years as radio frequency (RF) components and algorithms must yet mature and standardization still has to set the rules. In contrast, this work illustrates novel mmWave channel-as-a-sensor use cases, cf. Fig. 1, that can be realized sustainably by exploiting current 5G networks.

There have been multiple enhancements to the methods used to detect ground motion and to monitor infrastructure, however, expensive equipment and staff is yet prohibitive for many small-sized and funded applications. Our proposed system architecture complements existing measurement infrastructure for such applications as it enables dense deployment of sensors by reusing existing mmWave cellular infrastructure and mobile devices, and by leveraging the wireless channels in-between. In order to future-proof this solution, the envisioned sensing platform has to consist of precise, automated, fast, and intelligent systems. Our proposed method within this study, combined with the possibility of high data rates and reliable low latency data transmissions of 5G New Radio

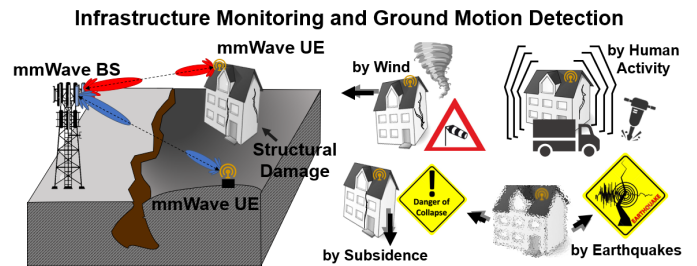


Fig. 1: Sensing of small-scale movements induced by natural (e.g. earthquakes, wind, waves) or anthropogenic (e.g. traffic, construction) sources of ground motion.

(NR) and associated edge computing capabilities for artificial intelligence (AI) analysis methods, is therefore proposed as a novel method for such sensing applications. By means of two examples we validate that our system will indeed be able to track 3D small-scale user equipment (UE) movements with μm -range accuracy.

The remainder of this paper is structured as follows. After discussing the need for mmWave sensing in Sec. II, we introduce novel use cases based thereon and discuss the envisioned system architecture in Sec. III. We then present the new measurement technique, the key part of the system, in Sec. IV. Last, we introduce our evaluation methodology in Sec. V and subsequently discuss the results of 3D ray-tracing based experiments in Sec. VI.

II. RELATED WORK: MMWAVE SENSING

While most design decisions for 6G sensing are yet up for debate, it is apparent that mmWave frequencies (> 24 GHz) will be exploited despite limitations in range reducing cell coverage to a few hundred meters [4]. Further, mmWave operation may be impacted by heavy rain, snowfall or vegetation. Hence, the inherent need of radar-like sensing for antenna sweeping contrasts the fine beam alignments required for mmWave communications and, together with multi-user requirements of operators for hotspot coverage, necessitates multi-beam capabilities of hybrid beamformers on network side [5]. However, the resulting transmit power sharing between the beams reduces the coverage, and introduces inter-beam interference which degrades sensing accuracy such that it must be compensated by well-designed beambooks.

Nonetheless, compared to sub-6 GHz sensing, the wider channels allow for better ranging resolution [6], and the

increased carrier frequency for better ranging accuracy [7] and velocity resolution [4]. Additionally, high path loss and low diffraction reduce the need for clutter suppression schemes [6]. Moreover, even small COTS drones can be detected with sufficient signal-to-noise ratio (SNR) in a range of about 250 m if pencil beams are facilitated [8]. These enable fine-grained angular sensing by means of their narrow beams [6], for example enabling very accurate positioning as shown in [9]. These beams also allow for suppression of interference and multipath at unwanted angles. Furthermore, multi-beam operation enables tracking of multiple targets at once [4]. Selective utilization of other beam pattern types, e.g. sector beams, further qualify mmWave transceivers as multi-mode sensors by being capable of fulfilling sensing requirements for long, medium and short range within just a single system, which is cheaper than using separate systems as in cars [10].

III. APPLICATIONS AND SYSTEM ARCHITECTURE FOR NOVEL 5G MMWAVE ENABLED APPLICATIONS

In this section we first derive the constraints for our novel 5G sensing use cases based on state-of-the-art mmWave communications and characterize the foreseen applications. Afterwards, we outline the perspectives 5G offers to the envisioned platform beyond the proposed measurement method.

A. mmWave Compatible Sensing Applications

5G NR (rel.-15/16) supports mmWave communications particularly by means of frequency range 2 (FR2) and beam management. Nowadays it is indeed possible to connect semi-stationary mmWave users to the network, but mmWave hardware and beam management are not yet mature enough to operate robustly throughout mobility. Consequently, we put our attention back to what is available right now, i.e. stationary base station (BS) and UE nodes and the acquired link in the form of CSI. Obviously, this does not enable the type of sensing in the scope of 6G, but nonetheless, ambient mobility will impact the link and this can be used to acquire context information, for example, by means of radio-fingerprints as shown in [11] at sub-6 GHz frequencies. As mmWave links are more prone to interrupts, such use cases are likely inapplicable. Hence, we introduce novel small-scale mobility scenarios that account for the previously discussed constraints as follows.

Novel Scenario: We envision an outdoor scenario, in which a mmWave UE is mounted on the exterior surface of the structure to be monitored, for example on the facade of a skyscraper. The mounting must ensure that there is a Line-of-Sight (LOS) path to the BS such that neither pedestrians nor vehicles are expected to interrupt the link; alternatively, specific Non-Line-of-Sight (NLOS) paths like ground or building reflections may suffice, too. With this setup the infrastructure is monitored for certain events, for example in the context of the discussed skyscraper setup, earthquakes and strong wind will particularly introduce small-scale mobility on UE side as it is mounted at high altitude compared to the mmWave BS which is typically near street level. As will be discussed later, the system may also be applied to subsidence scenarios and, in future, enable tracking of all kinds of movements.

1) *Use Cases and Characteristics:* In this section we investigate the characteristics of seismicity, wind and weather, and subsidence in order to identify the requirements for sensing.

a) *Seismic Ground Motion:* Human activities and natural events alter the stresses and strains in the earth's crust, eventually leading to the release of seismic waves traveling through the earth or along the earth surface (body/surface waves). Body waves can be subdivided into primary and secondary waves, both traveling at speeds of several 1,000 m/s, where P-waves travel quicker and with less energy; surface waves have a much lower velocity. In addition, any motion at the surface generates waves traveling in the subsurface, e.g. atmospheric pressure fluctuations and scattering of ocean waves [12]. Reported frequencies are typically in the range of 0.05 Hz to 1 kHz, where higher frequency signals are often generated by anthropogenic sources and local earthquakes are detected in the range of 0.5-20 Hz. Surface waves from distant earthquakes can have periods of tens of seconds [13], [14].

b) *Wind and Weather:* In [15], horizontal movement of a skyscraper in the range of about 30 mm was detected at an altitude of about 200 m. The key wind-induced oscillation frequencies were 0.48 Hz and 0.60 Hz at weak wind with velocity of about 5-9 m/s. Particularly during strong storms it is essential to track such movement to assess and predict the risk of structural instability in real-time.

c) *Subsidence:* Mining regions around the world suffer from subsidence, i.e. sudden sinking or gradual downward settling of the ground with little to no horizontal motion. This also occurs where petroleum, gas or groundwater is extracted. There are also natural reasons for subsidence, e.g. erosion and earthquakes, which lead to the formation of cracks in infrastructure accompanied by structural damages. Typical values for gradual settling are within a couple of millimeters per year, e.g. 2.1-3.4 mm/year [16].

2) *Impact on Channel:* In this section we review the impacts of the introduced events on mmWave links.

a) *Wireless:* So far, analysis of Free Space Optics (FSO) [17] and sub-6 GHz [18] links provide conflicting results on the applicability of received signal strength (RSS) measurements for earthquake detection. The considered frequencies, however, exhibit significantly different propagation characteristics than at mmWaves. Beam misalignments studied in [19] showed that the RSS may degrade significantly, however, they were larger than expected for our use cases.

b) *Wired:* In the area of fiber optic communications it has been demonstrated in [13] that ground motion can be detected and analyzed resolving the phase of backscattered photons along the optical fiber by using high precision equipment not applicable to wireless communications.

B. System Architecture

At last, we consider the enhancements our concept offers to the respective sectors to better assess the previously discussed events. Further, it can also be used to raise alarms such that people in risk can evacuate and prepare for the disaster event,

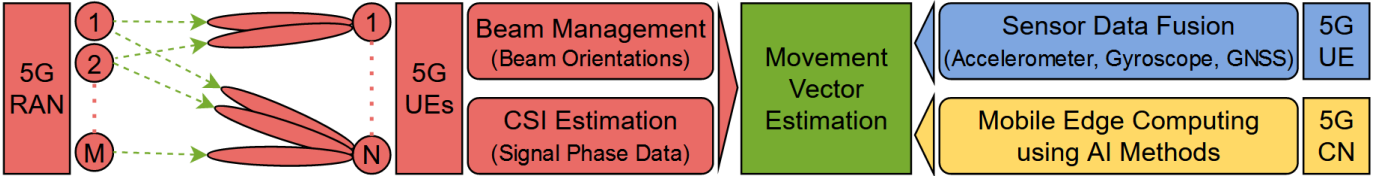


Fig. 2: Envisioned 5G mmWave sensing system. This work investigates movement estimation based on the red function blocks.

or be rescued more easily. Our suggested method for this, cf. Sec. IV, is part of a larger platform shown in Fig. 2.

Our concept embeds handy, easy-to-install measurement platforms into existing 5G networks and thus allows for seamless connectivity. Novel radio interferometry methods for structural dynamic studies now allow for detection of small strains and deformations from afar using two specifically arranged antennas; our method may be interpreted as an adaptation of this concept to cellular networks. Classical measurements use various methods such as inertial sensors, strainmeters or gyroscopes [14], which may also be considered with the envisioned platform as COTS 5G devices have similar in-built sensors. Another such example is global navigation satellite system (GNSS)-based sensing, however, this is easily obstructed [20]. There are more arguments for the system:

1) *mmWave Smartphones*: In recent years, there has been an increasing demand for integration and usage of monitoring systems from small to big scales, however, these require expensive equipment and professional staff, leading to less application in medium to small-sized and funded processes. For example, the analysis of seismic signals historically relied on the detection of specific events at different stations for source localization and analysis of subsurface rock formation properties. In the past two decades, however, it has been shown that diffuse waves traveling in all directions can produce a point source in the medium which can be used to study the subsurface medium [12]. However, in urban environments waves typically have a directionality depending on prominent noise sources such as trains. Using mobile phones for localization of such noise sources can help transform formerly unspecified noise from anthropogenic activities to distinct sources of seismic energy. This becomes a feasible option as 5G mmWave UEs are set to be ubiquitously available, thus enabling dense and broad deployment of sensors and becoming part of future smart cities.

2) *AI Applications*: The discussed method in this study is based on a monitoring system providing large datasets of complex variables from different sensors and platforms compared to conventional methods. This results in complexities difficult to solve by standard numerical techniques alone. The use of novel AI methods such as deep learning and physics-informed machine learning (ML) models could have a tremendous enabling impact on analyzing the obtained data. Using these, embedment into 5G networks enables fast and efficient computation within the mobile edge cloud of the operator. Hence, the goal of identifying the state and actual behavior of studied structures may be reached sustainably, and further allows for better-informed decisions.

IV. PROPOSED MMWAVE MEASUREMENT TECHNIQUE

Based on our previous discussion, we introduce our concept which enables fine monitoring and tracking of small-scale mobility over any period of time.

For this we use the signal phase information comprised within the channel estimate vector $\widehat{H}(f)$ for time instances t , which is available at N out of at maximum 3,300 different orthogonal frequency-division multiplex (OFDM) subcarriers $f = f_0 + n \cdot \Delta f, n = 0, 1, \dots, N - 1$, of 5G NR ($N \ll 3,300$), where f_0 is the mmWave carrier and Δf depends on numerology and CSI Reference Signal (CSI-RS)¹ density in frequency domain [21]. In the following derivation we assume that $\widehat{H}(f)$ is acquired *a*) at a rate suiting the use case, e.g. in the range of kHz for earthquakes to minute intervals for subsidence², and *b*) using a bandwidth $N \cdot \Delta f$ sufficient for a movement monitoring with predetermined accuracy of the use case³.

Once the UE moves, the signal phases change from measurement $\widehat{H}_{\text{ref}}(f)$ at $t = t_0$ to $\widehat{H}_{\text{shift}}(f)$ at $t = t_1 > t_0$, hence

$$\delta(f) = \angle \widehat{H}_{\text{shift}}(f) - \angle \widehat{H}_{\text{ref}}(f), \delta \in (-180, 180]^\circ. \quad (1)$$

After unwrapping phase differences $\delta(f)$ over vector f , the movement can be estimated at each subcarrier individually by

$$d(f) = \frac{\delta_{\text{unwrapped}}(f)}{180^\circ} \cdot \frac{c_0}{f}, \quad (2)$$

where c_0 stands for the speed of light. Finally, a scalar estimate of the relative movement between the two sensor locations is derived from vector $d(f)$ using $\widehat{d} = \text{mean}(d(f))$ or a more sophisticated estimator. We note that \widehat{d} could be determined in time domain using the phase of the strongest channel impulse response (CIR) tab, which mitigates the estimation error in \widehat{d} due to multipath, but time resolution will be crucial.

However, estimate \widehat{d} only corresponds to the movement along the axis of the incident electromagnetic (EM) wave. As illustrated in [15], the corresponding movement in Cartesian coordinates can be recovered if the angle of the incident wave is known. Fortunately, 5G NR mmWave transceivers can determine these on their own based on their beamsteering capability⁴, either from beam training or later refinement, e.g. using SSs, CSI-RSs or PRSs. Considering the azimuth and elevation angles $\phi \in (-180, 180]^\circ, \theta \in [-90, 90]^\circ$, cf. Fig. 3a, the UE recovers the movement as follows (extending [15]):

$$\left(\widehat{\Delta x}, \widehat{\Delta y}, \widehat{\Delta z} \right)^T = \widehat{d} \cdot \left(\frac{\cos(\phi)}{\cos(\theta)}, \frac{\sin(\phi)}{\cos(\theta)}, \frac{1}{\sin(\theta)} \right)^T. \quad (3)$$

¹Other 5G NR signals such as synchronization signals (SSs) or rel-16 positioning reference signals (PRSs) could be exploited in addition to CSI-RS.

²CSI-RS may be configured periodic (every M^{th} slot with $M \in [4, 640]$, enabling velocity estimation) or aperiodic (on demand). Considering the minimal FR2 slot length of 125 μs , sampling rates up to 2 kHz are supported [21].

³CSI-RS may cover only fractions of the carrier bandwidth part (BWP) [21].

⁴Classical angle finding algorithms, e.g. MUSIC, may also be considered.

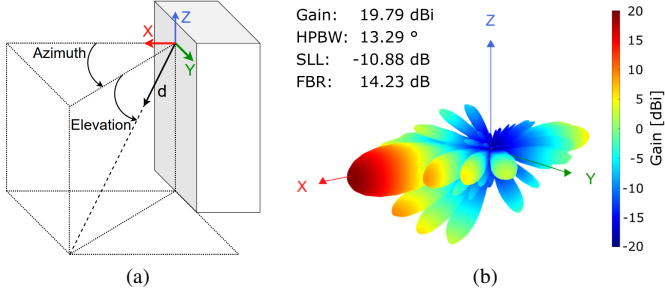


Fig. 3: (a) Illustrated setup of a wall-mounted UE aligning pencil beam to incident mmWaves (here: pos. ϕ , neg. θ). (b) Simulated pencil beam pattern with $(\phi, \theta) = (0, 0)^\circ$.

This estimate, however, couples the components and might therefore suffer from errors. Nonetheless, this system is suited to detect an initial movement \hat{d} with a single UE and moreover able to provide an initial estimate of its (x, y, z) components.

A. Improving Sensing Performance

Upon confirmation of such an initial movement event, fine-grained 3D tracking of the movement with better accuracy might be desired to assess the movement over time. For this purpose, the data of the previous process (up to Eq. 3) could be fused with accelerometer and gyroscope sensor data. Another possibility comes from using several mmWave links, either between a single UE and several BSs or between several UEs and serving BS. In the following section, we investigate the latter option as it offers the customer flexibility in deployment.

If $U \geq 3$ is the overall number of deployed UEs, \hat{d}_u for $u = 1, \dots, U$ are measured along beam orientations

$$\vec{r}_u = (\cos(\theta_u) \cos(\phi_u), \cos(\theta_u) \sin(\phi_u), \sin(\theta_u))^T. \quad (4)$$

Analogously to velocity vector estimation from radial velocity measurements with several radars [22], the movement vector is reconstructed in three steps. First, two mutually orthonormal vectors $\vec{o}_{A,u}, \vec{o}_{B,u}$ are determined for each \vec{r}_u vector. Second, the equation system $\vec{b} = A \cdot \vec{c}$ describing the point of intersection of U planes in space is set up with column vector \vec{b} of length $3(U-1)$ and matrix A as follows (here: $U = 3$).

$$\vec{b} = \begin{pmatrix} \hat{d}_2 \cdot \vec{r}_2 - \hat{d}_1 \cdot \vec{r}_1 \\ \hat{d}_3 \cdot \vec{r}_3 - \hat{d}_1 \cdot \vec{r}_1 \end{pmatrix} \quad (5)$$

$$A = \begin{pmatrix} \vec{o}_{A,1}, \vec{o}_{B,1}, -\vec{o}_{A,2}, -\vec{o}_{B,2}, 0_{3 \times 1}, 0_{3 \times 1} \\ \vec{o}_{A,1}, \vec{o}_{B,1}, 0_{3 \times 1}, 0_{3 \times 1}, -\vec{o}_{A,3}, -\vec{o}_{B,3} \end{pmatrix} \quad (6)$$

After determining column vector \vec{c} of length $2U$ using the inverse⁵ of A , the small-scale movement is reconstructed at last using tuples of its coefficients $\hat{c}_i, i = 1, \dots, 2U$:

$$\begin{pmatrix} \hat{\Delta x}_u, \hat{\Delta y}_u, \hat{\Delta z}_u \end{pmatrix}^T = \hat{d}_u \cdot \vec{r}_u + \hat{c}_{2u-1} \cdot \vec{o}_{A,u} + \hat{c}_{2u} \cdot \vec{o}_{B,u}. \quad (7)$$

Considering system scalability, we determine the final $\hat{\Delta x}, \hat{\Delta y}$ and $\hat{\Delta z}$ values using the mean of all U outcomes of Eq. 7.

V. METHODOLOGY

In this section we introduce the methodology to evaluate the proposed concept as follows. In Sec. A, we set up the ray-tracing simulation tool with regard to the CSI-RS configuration

⁵Pseudo-inverse $(A^T A)^{-1} A^T$ finds the least squares solution if $U > 3$.

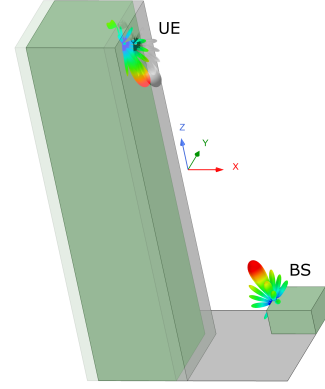


Fig. 4: Urban scenario (colorized) with induced movement (shaded) along positive x-axis of skyscraper-mounted UE $[\rightarrow]$.

and mmWave antenna beam pattern. We then introduce two scenarios representing different use cases in Sec. B-C. Sec. D extends these setups to multiple UEs. Last, Sec. E gives a brief overview of the performance metrics used in Sec. VI.

A. Ray-Tracing: CSI-RS Configuration and Antenna Setup

Our evaluation is based on 3D ray-tracing data from [23], which allows for modelling of mmWave channels considering fine-grained, parametrized movements using the shooting and bouncing ray (SBR+) solver. The 5G network operates in FR2 band n257 at $f_0 = 26.5$ GHz leveraging 400 MHz of bandwidth. Considering both CSI-RS density of 1 and 60 kHz numerology, the ray-tracer calculates $N = 555$ channel samples with $\Delta f = 720$ kHz spacing⁶. Using [24] we have further designed an 8×8 uniform planar array (UPA) consisting of 64 patch antennas at half-wavelength spacing. We provide the boresight beam pattern in Fig. 3b along with the following key parameters: maximum antenna gain, half-power bandwidth (HPBW), sidelobe level (SLL) and front-to-back ratio (FBR).

B. Skyscraper Scenario

The first scenario depicted in Fig. 4 is an example of infrastructure monitoring (e.g. wind, seismicity). The mmWave BS is mounted near pedestrian level (height: 10 m) on the outside of a building ($20 \times 20 \times 12$ m) whereas the UE is mounted 150 m higher up on the facade of a skyscraper ($40 \times 40 \times 170$ m); the horizontal spacing of the sites is 30 m along x- and y-axes, respectively. Considering this setup, the beams are aligned optimally with $(\phi, \theta) = (45.0, -78.7)^\circ$ (UE side). The simulated small-scale movements of skyscraper and UE are along the x-axis with $x_{\text{shift}} = 0, 1, \dots, 5$ mm.

C. Subsidence Scenario

The second scenario, as shown in Fig. 5, considers subsidence affecting a suburban house and the mounted UE along the z-axis with $z_{\text{shift}} = 0, -1, \dots, -5$ mm. The BS is mounted at an height of 10 m on the outside of a community center ($20 \times 20 \times 12$ m) whereas the UE is mounted at 4 m altitude on the facade of the customer's house ($10 \times 10 \times 6$ m); the horizontal separation of the devices are 15 m and 30 m along x- and y-axes, respectively. For this setup, optimal beam alignment is achieved by $(\phi, \theta) = (63.4, 10.1)^\circ$ on UE side.

⁶This setup neglects guard bands and requires carrier aggregation.

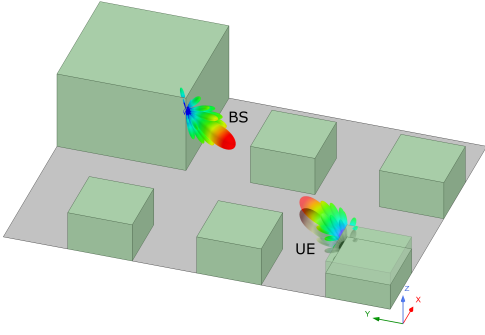
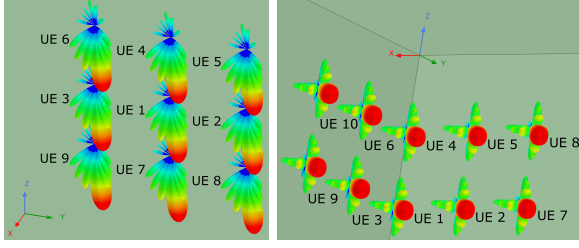


Fig. 5: Implemented suburban scenario (colorized) exhibiting subsidence (shaded) along negative z -axis of UE [↓].



(a) Skyscraper (9 UEs). (b) Subsidence (10 UEs).

Fig. 6: Multi-UE Deployments of Scenarios (a) and (b).

D. Deployment of Multiple UEs

Considering Sec. IV-A, simulation and evaluation consider deployments of up to 10 UEs with ideally aligned beams as shown in Fig. 6. The additional UEs are mounted next to reference UE 1 following the illustrated axes in steps of 1 m.

For our evaluation in Sec. VI we particularly consider multi-UE deployments using ≥ 3 UEs. Analyzing all possible deployment constellations in detail exceeds the scope of this paper, hence we select those minimizing the condition number (CN) $\|A^{-1}\|_2 \cdot \|A\|_2$ of matrix A for a given U based on its relative error (RE) limiting characteristic described in [25].

E. Evaluation Metrics

a) *Specific UE Constellation:* In Sec. VI, we first compare several movement vector estimates $\vec{m}_{\text{meas}} = (\widehat{\Delta x}, \widehat{\Delta y}, \widehat{\Delta z})$ component-wise to the true movement $\vec{m}_{\text{move}} = (x_{\text{shift}}, 0, 0)$ or $(0, 0, z_{\text{shift}})$, respectively, for increasing absolute shift. This comparison uses the results of single UE 1 on the one hand, and of $U = 3, 4, 6$ and 9 UE deployments on the other hand. Second, we investigate the RE = $\|\vec{m}_{\text{meas}} - \vec{m}_{\text{move}}\|_2 / \|\vec{m}_{\text{move}}\|_2$. We compare the incurred REs of UE 1 by itself as well as for multi-UE deployments using $U = 3, \dots, 9$ UEs at once.

b) *Performance Distribution:* Last, we determine the mean RE of any UE constellation over x_{shift} and z_{shift} , respectively. Using the mean REs of all constellations, we derive the empirical cumulative distribution function (ECDF) of mean RE and compare the ECDFs for $U = 3, \dots, 9$.

VI. EVALUATION

A. Evaluation of Skyscraper Scenario

Fig. 7 compares the estimates of the multi-UE setups with minimal CN to the ones of reference UE 1. It can be seen that

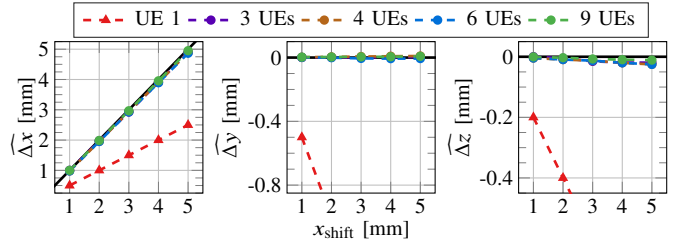


Fig. 7: Measured vs. true movement of skyscraper scenario.

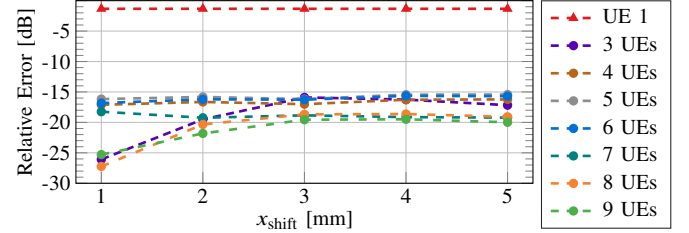


Fig. 8: RE of movement measurement of skyscraper scenario.

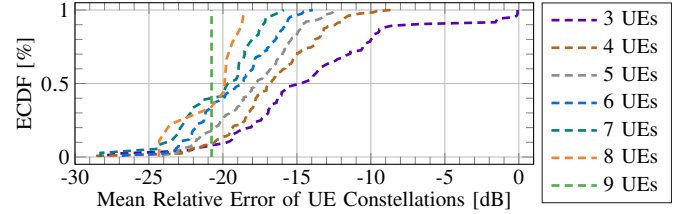


Fig. 9: Distribution of mean RE in skyscraper scenario.

the multi-UE measurements approach the ideal performance, although there is still a discernible error, cf. $\widehat{\Delta z}$ over x_{shift} . However, compared to the single UE setup, the error for all movement components has been reduced. This can further be seen in Fig. 8 illustrating the incurred REs which have been reduced by at least 14.3 dB. With RE < -15 dB in all cases, accuracy is better than $32 \mu\text{m}$; sometimes even better than $10 \mu\text{m}$ (RE < -20 dB), likely depending on multipath.

Considering Fig. 9 showing the distribution of mean RE over all possible multi-UE constellations for $U = 1, \dots, 9$, it can be seen that the minimal CN constellations considered previously are not the best performing ones, however, still far from being the worst. Compared to Fig. 8 it can clearly be seen that increasing U increases the likelihood for deploying an UE constellation with increased measurement accuracy such that it approaches $1 \mu\text{m}$ in the best case. It can also be seen that deployments of 3 UEs can perform very inaccurate; this is due to UE constellations for which matrix A is ill-conditioned (here: 1-norm CN $\geq 10^{12}$) forcing use of the pseudo-inverse.

B. Evaluation of Subsidence Scenario

As the results for this scenario are even better than in Sec. VI-A, we limit the evaluation to the ECDF of mean RE shown in Fig. 10. In this setup nearly all deployments with more than three UEs (96.2-100%) offer sub- $10 \mu\text{m}$ accuracy throughout z_{shift} , with some again approaching micrometer accuracy. This contrasts the mean RE of -7.5 dB for single UE 1. A reason for this performance enhancement could

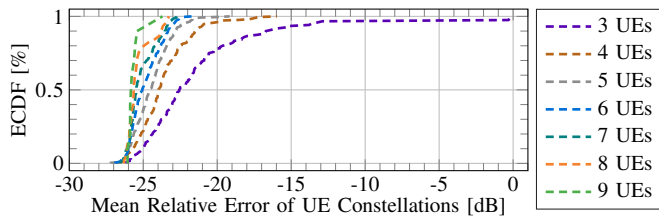


Fig. 10: Distribution of mean RE in subsidence scenario.

be the reduced scenario size translating to increased azimuth and elevation ranges being covered by the UEs, i.e. $(\Delta\phi, \Delta\theta) = (4.4, 3.5)^\circ > (1.9, 0.7)^\circ$, and thus providing more 3D movement information. However, the accuracy gain of adding UEs has shrunk as the ECDFs are overall spaced more tightly than in Fig. 9, thus making the placement of UEs a key optimization step before deployment, e.g. by using 3D environment maps. Further, when recalling the envisioned deployments of a single UE exploiting several propagation paths to one or more BSs, this shows that even with expected numbers of up to 4-5 distinct mmWave link opportunities per BS [19], sensing accuracy might indeed be very good.

VII. CONCLUSIONS

Sensing is expected to be a key topic for 6G standardization, but the envisioned use cases are far from realizable right now. In contrast, this work has introduced the sustainable secondary use of 5G mmWave for ground motion sensing and infrastructure monitoring, for research and safety purposes, using COTS UEs. For a lightweight deployment, a single UE is able to detect small-scale movement by evaluating CSI phase changes. After detection of such an event, deployment of multiple UEs, all of which align their beams using known beam management procedures, allows for precise reconstruction of 3D movement using movement vector estimation. By means of ray-tracing based experiments we have verified that the achievable 3D movement tracking error is well below $10 \mu\text{m}$.

Our ongoing research is investigating the performance of the proposed single UE deployment option which leverages several available, distinct multipath opportunities to the mmWave network at once. We are currently also studying the system performance under error sources such as noise and beam misalignments to validate our results. Future works will integrate on-board sensor data and AI methods, and may further investigate the impact of UE placement or application-based physical resource demands. Moreover, we plan to extend our framework to leverage movement-caused angular changes and phase-based ranging. Last, in the context of 6G joint communication and radio/radar sensing (JCAS), we aim to study the applicability of our concept to study objects from afar, i.e. without UEs.

ACKNOWLEDGMENT

This work has been supported by the Ministry of Economic Affairs, Innovation, Digitalization and Energy of the State of North Rhine-Westphalia (MWIDE NRW) along with the Competence Center 5G.NRW under grant number 005-01903-0047, and by the German Research Foundation (DFG) within the Collaborative Research Center SFB 876 "Providing Information by Resource-Constrained Analysis," project A4.

REFERENCES

- [1] A. Bourdoux *et al.*, "6G White Paper on Localization and Sensing," *arXiv eess.SY e-prints*, Jun. 2020.
- [2] J. A. Zhang *et al.*, "Perceptive mobile networks: Cellular networks with radio vision via joint communication and radar sensing," *IEEE Vehicular Technology Magazine*, Jun. 2021.
- [3] A. Ali *et al.*, "Leveraging sensing at the infrastructure for mmWave communication," *IEEE Comm. Mag.*, vol. 58, no. 7, 2020.
- [4] M. Alloulah and H. Huang, "Future millimeter-wave indoor systems: A blueprint for joint communication and sensing," *Computer*, vol. 52, no. 7, 2019.
- [5] J. A. Zhang *et al.*, "Multibeam for joint communication and radar sensing using steerable analog antenna arrays," *IEEE Transactions on Vehicular Technology*, vol. 68, no. 1, 2019.
- [6] F. Liu *et al.*, "Joint radar and communication design: Applications, state-of-the-art, and the road ahead," *arXiv eess.SP e-prints*, Jun. 2019.
- [7] A. Bhutani *et al.*, "The role of millimeter-waves in the distance measurement accuracy of a FMCW radar sensor," *Sensors*, vol. 19, no. 18, 2019.
- [8] Y. Wang *et al.*, "28 GHz 5G-based phased-arrays for UAV detection and automotive traffic-monitoring radars," in *2018 IEEE/MTT-S International Microwave Symposium*, 2018.
- [9] K. Heimann, J. Tiemann, S. Böcker, and C. Wietfeld, "Cross-bearing based positioning as a feature of 5G millimeter wave beam alignment," in *IEEE 91st Vehicular Technology Conference (VTC2020-Spring)*, 2020.
- [10] J. Hasch *et al.*, "Millimeter-wave technology for automotive radar sensors in the 77 GHz frequency band," *IEEE Transactions on Microwave Theory and Techniques*, vol. 60, no. 3, 2012.
- [11] B. Sliwa, N. Piatkowski, and C. Wietfeld, "The channel as a traffic sensor: Vehicle detection and classification based on radio fingerprinting," *IEEE Internet of Things Journal*, vol. 7, no. 8, 2020.
- [12] R. Snieder and K. Wapenaar, "Imaging with ambient noise," *Physics Today*, vol. 63, no. 9, 2010.
- [13] P. Jousset, T. Reinsch, T. Ryberg, H. Blanck, A. Clarke, R. Aghayev, G. Hersir, J. Hennings, M. Weber, and C. Krawczyk, "Dynamic strain determination using fibre-optic cables allows imaging of seismological and structural features," *Nature Communications*, vol. 9, no. 2509, 2018.
- [14] D. C. Agnew, "Seismic instrumentation," in *Encyclopedia of Solid Earth Geophysics*, H. K. Gupta, Ed. Cham: Springer International Publishing, 2021, pp. 1419–1425.
- [15] M. Talich, "Monitoring of horizontal movements of high-rise buildings and tower transmitters by means of ground-based interferometric radar," *The International Archives of the Photogrammetry, Remote Sensing and Spatial Information Sciences*, vol. XLII-3/W4, 2018.
- [16] P.-Y. Declercq *et al.*, "Long-term subsidence monitoring of the Alluvial plain of the Scheldt river in Antwerp (Belgium) using radar interferometry," *Remote Sensing*, vol. 13, no. 6, 2021.
- [17] M. Matsumoto *et al.*, "Innovative tracking system for next generation FSO systems under massive earthquakes," in *2015 International Conference on Optical Network Design and Modeling*, 2015.
- [18] J. Nachtigall *et al.*, "The challenges of using wireless mesh networks for earthquake early warning systems," in *2009 Second International Conference on Advances in Mesh Networks*, 2009.
- [19] L. Grannemann *et al.*, "Urban outdoor measurement study of phased antenna array impact on millimeter-wave link opportunities and beam misalignment," *IEEE Trans. on Wireless Comm.*, vol. 20, no. 3, 2021.
- [20] N. Houlié *et al.*, "New approach to detect seismic surface waves in 1Hz-sampled GPS time series," *Scientific Reports*, vol. 1, p. 44, 07 2011.
- [21] E. Dahlman, S. Parkvall, and J. Skold, *5G NR: The Next Generation Wireless Access Technology*, 1st ed. USA: Academic Press, Inc., 2018.
- [22] B. Nuss, Y. L. Sit, and T. Zwick, "3D radar image fusion using OFDM-based MIMO radar," in *2016 German Microwave Conf. (GeMiC)*, 2016.
- [23] Ansys Inc., "Ansys HFSS SBR+," available: <https://www.ansys.com/content/dam/resource-center/application-brief/ansys-sbr-plus.pdf> [last visited: September 29, 2021].
- [24] Ansys Inc., "Ansys HFSS for Antenna Simulation," available: <https://www.ansys.com/content/dam/product/electronics/hfss/ab-ansys-hfss-for-antenna-simulation.pdf> [last visited: September 29, 2021].
- [25] C. Moler, "What is the condition number of a matrix?" available: <https://blogs.mathworks.com/cleve/2017/07/17/what-is-the-condition-number-of-a-matrix/> [Last visited: September 29, 2021].